A EUROPEAN JOURNAL

CHEMPHYSCHEM

OF CHEMICAL PHYSICS AND PHYSICAL CHEMISTRY

Accepted Article

Title: Tuning the Optical Properties of Sulfonylaniline Derivatives: Degeneracy Breaking of Benzene Orbitals and Linkage Through Nodal Planes

Authors: Shoh Kudo, Nanami Hoshino, Teruo Beppu, and Hiroshi Katagiri

To be cited as: *ChemPhysChem* 10.1002/cphc.201900135

Link to VoR: http://dx.doi.org/10.1002/cphc.201900135

A Journal of ChemPubSoc Europe

WILEY-VCH www.chemphyschem.org

10.1002/cphc.201900135

WILEY-VCH

ARTICLE

Tuning the Optical Properties of Sulfonylaniline Derivatives: Degeneracy Breaking of Benzene Orbitals and Linkage Through Nodal Planes

Shoh Kudo, Nanami Hoshino, Teruo Beppu, and Hiroshi Katagiri*[a]

Abstract: The orbital degeneracy of benzene rings is resolved by an asymmetric push-pull system in 2,6-bis(methylsulfonyl)aniline (BMeSA), in which the highest occupied molecular orbital (HOMO) is located at the 4-position, while the lowest unoccupied molecular orbital (LUMO) is located at a different position and has a nodal plane through the carbon atoms at the 1- and 4-positions. Therefore, the π-extension of BMeSA at the 4-position reveals a strong overlap in the HOMO and a minimal overlap in the LUMO. Consequently, π-extended BMeSA derivatives exhibit longer absorbance and emission wavelengths in the order of the electron-donating abilities of their substituents at the 4-position, which is based on a decrease in an absolute HOMO-level-dependent HOMO-LUMO gap in accordance with the nodal arrangement. Positive fluorescent solvatochromism with polarity-dependent decrease in fluorescent intensity was also observed. The biaryls exhibited more planar geometries in the excited state than in the ground state. The charge transfer mechanism, which can be described as node-induced intramolecular charge transfer (NICT), differs from the planar intramolecular charge transfer (PICT) and twisted intramolecular charge transfer (TICT).

Introduction

π-Conjugated small molecules have been in the limelight of organic optoelectronic materials research for years now, because of their potential biosensing[1,2] and optoelectronic applications.[3-6] Various combinations of aromatic skeletons and substituent effects can be adopted in the construction of π-conjugation systems. However, a rational paradigm for their molecular design is still lacking; therefore, new concepts need to be developed. Since conversancy with the highest occupied molecular orbital (HOMO) and lowest unoccupied molecular orbital (LUMO) is essential in understanding the optical properties of molecules, controlling their energy levels and distributions will be of significance in designing π-conjugated molecules in the future.[7]

[a] *S. Kudo, N. Hoshino, T. Beppu, Prof. Dr. H. Katagiri*
Graduate School of Science and Engineering
Yamagata University
4-3-16 Jonan, Yonezawa, Yamagata 992-8510, Japan
E-mail: kgri7078@yz.yamagata-u.ac.jp

Supporting information for this article is available on the WWW under http://dx.doi.org/xxxxx. It contains NMR and HRMS spectra of novel compounds, peak separation data, X-ray crystallographic data, and DFT calculation details.

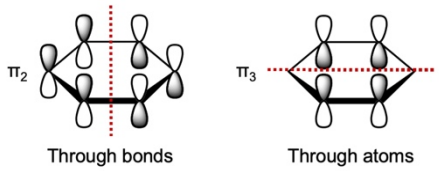

Figure 1. Representation of the two types of nodal planes on the two molecular orbitals of benzene (π_2 and π_3) which have the same energy and are degenerate.

The nodal plane, where the probability of finding an electron is zero, is divided into two types: the nodal plane through bonds and the nodal plane through atoms (Figure 1). The latter is particularly important for π-conjugated molecules because the linkage through the nodal plane enables the control of optical properties via overlapping or non-overlapping of the frontier orbitals in π-conjugation systems. Simple hydrocarbons such as pyrene, fluorene, s-indacene, and azulene have potentially useful architectures; their nodal planes, which cut through atoms with free sites, are available for chemical modification. For example, pyrene oligomers with a linkage through their nodal planes, which serve as individual radical ion building blocks for organic magnetic materials;[8] the control of charge recombination in dye-sensitized solar cells using the orbital symmetries and nodal planes of azulene, pyrene, and fluorene derivatives;[9] terazulenes, for controlling the charge carrier polarity in organic transistors through controlling the molecular orbital distribution;[10,11] and fine-tuning the HOMO and LUMO energies of pyrene derivatives through modifications at the free sites on the nodal plane.[12-15] Several recent studies have focused on frontier orbital overlaps and their nodal arrangements, which are important for promoting large-scale electronic coupling in macromolecules and for self-assembly.[16-19] Conversely, ordinary symmetrical aromatics such as benzene have no nodal plane through their atoms, because orbitals with the same energy are degenerate. Therefore, an asymmetric arrangement of electron donors or acceptors is necessary to disrupt the orbital degeneracy of benzene to generate a nodal plane. In this study, based on our previous concept of a push–pull system between amino and sulfonyl moieties,[20,21] 2,6-bis(methylsulfonyl)aniline (BMeSA) exhibits an asymmetric HOMO-LUMO distribution (Figure 2a), in which the HOMO is located at the 1- and 4-positions, while the LUMO, which is located at a different position, instead, generates a nodal plane through the atoms at the 1- and 4-positions. BMeSA-Ar **1a-d** (Figure 2b), which are π-extended derivatives at the 4-position of

BMeSA, exhibit HOMO-dependent tuning of the optical properties, a large dipole moment in the excited state, and positive solvatochromism in fluorescence spectra with a large Stokes shift based on asymmetric molecular orbital distribution and linkage through the nodal plane.

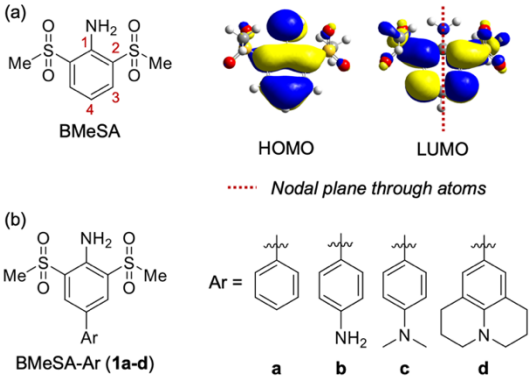

Figure 2. (a) Schematic representation of 2,6-bis(methylsulfonyl)aniline (BMeSA) with the asymmetric frontier orbitals and nodal plane through atoms. (b) BMeSA-Ar: π-extended derivatives at the 4-position of BMeSA.

Results and Discussion

Preparation of BMeSA and its π-extended derivatives, BMeSA-Ar(1a-d). BMeSA and its π-extended derivatives, BMeSA-Ar**(1a-d)**, were prepared through the synthetic route shown in Scheme 1. BMeSA was synthesized in three steps from 2,6-difluoronitrobenzene, **2**: a nucleophilic aromatic substitution of the methanethiolate on **2** afforded sulfide, **3**; catalytic hydrogenation with palladium on carbon reduced the nitro group; subsequent oxidation with *m*CPBA afforded good yields of BMeSA. Notably, the bromination of BMeSA using *N*-bromosuccinimide (NBS) proceeded selectively and afforded the 4-bromo derivative, **5,** in quantitative yield. Subsequently, Suzuki−Miyaura cross-coupling of **5** with the corresponding boronic acid esters, **6a-d,** afforded the desirable BMeSA-Ar (**1a-d**) in moderate to good yields. The full structures of the final BMeSA and BMeSA-Ar (**1a-d**) compounds were determined by single-crystal X-ray diffraction. The details of the syntheses and characterizations of the novel compounds are described in Figures S1-8 in Supplementary Data.

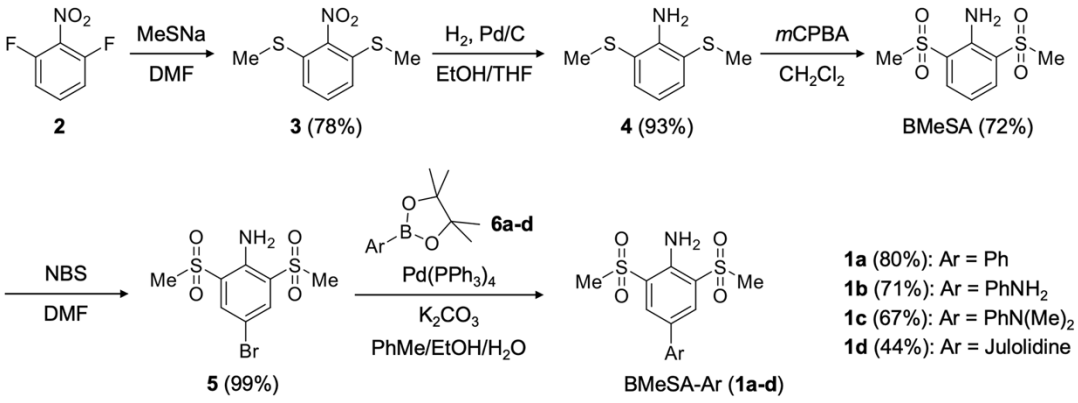

Scheme 1. Synthetic route to BMeSA and its π-extended derivatives, BMeSA-Ar.

***Theoretical calculations on BMeSA and BMeSA-Ar*(1a-d).** Density functional theory (DFT) and time-dependent density functional theory (TDDFT) calculations were performed on BMeSA and BMeSA-Ar (**1a-d**) using the polarizable continuum model (PCM) to investigate the frontier molecular orbital distributions, orbital energies, absorption spectra, and fluorescent spectra, in dichloromethane. The geometry optimizations were performed using the respective crystal structures as the initial geometries, and the resulting conformations for all molecules were in good agreement with those of the crystal structures (except for **1d**, because its methylsulfonyl groups assumed *syn* conformation in single crystals and *anti* conformation was adopted in the calculation, which was the same for other molecules).

As shown in Figure 3, the molecular orbital distribution of the LUMO included the nodal plane through the atoms at the 1- and 4-positions of the BMeSA moiety in all molecules. Therefore, in all the molecules, the LUMO was located in the BMeSA moiety without orbital overlap; the HOMO of all the molecules were distributed over the entire molecule with a large orbital overlap between the 1- and 4-positions. Moreover, the HOMO energies drastically increased in the order of BMeSA (–6.57 eV) < **1a** (–6.22 eV) < **1b** (–5.60 eV) < **1c** (–5.29 eV) < **1d** (–5.10 eV) relative to the electron-donating abilities of the aryl groups, whereas the LUMO energies were nearly the same in these molecules. Accordingly, the HOMO-LUMO energy gaps decreased in the order of BMeSA > **1a** > **1b** > **1c** > **1d**. The interplanar angles of the biphenyl groups of **1a-d** are in the range of 143.0°-146.6°, all of which are acceptable values for the orbital overlap between two benzene rings. The results of these calculations suggest the potential for controlling the HOMO-level-dependent energy gap based on the strong orbital overlap in the HOMO and the minimal orbital overlap in the LUMO.

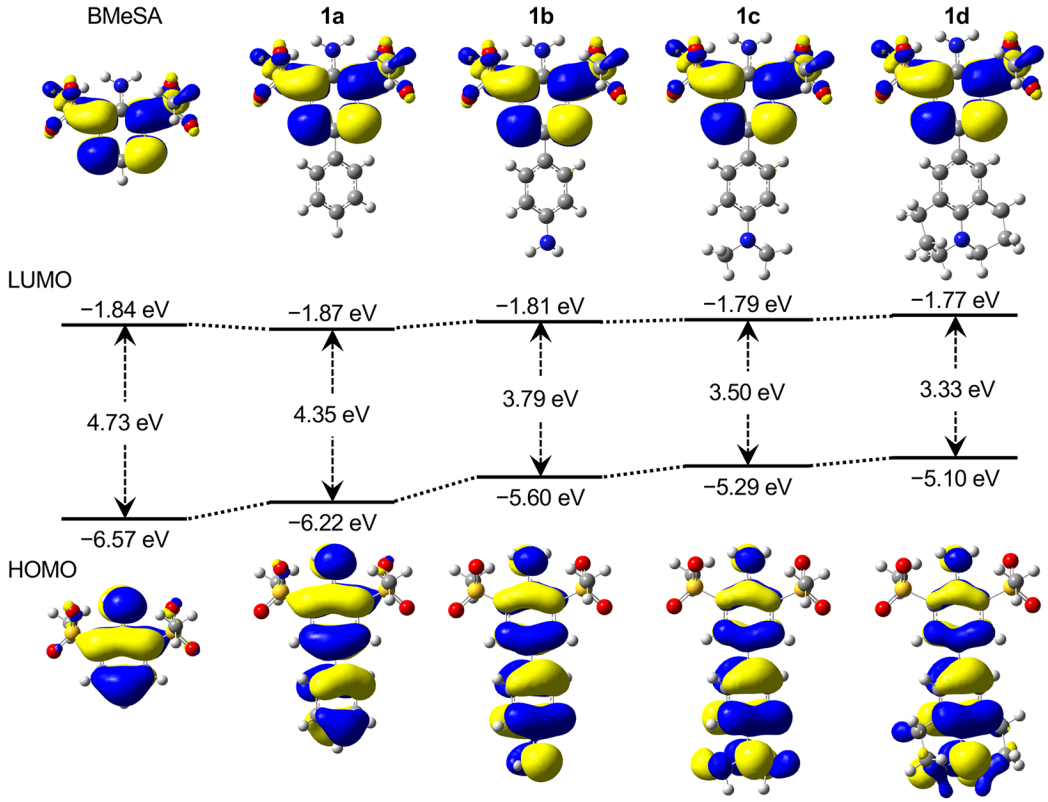

Figure 3. Optimized geometry, frontier molecular orbitals, and orbital energies of BMeSA and BMeSA-Ar (**1a-d**) in the ground state. Dichloromethane was used as the solvent for calculations (polarizable continuum model) at the B3LYP/6-31+G(d,p) level.

Table 1. Calculated absorption and fluorescence properties of BMeSA and BMeSA-Ar (**1a-d**) in dichloromethane.

	Absorption[a]			Fluorescence[b]		
	λ^{max}_{abs} [nm]	Oscillator strength	Contribution[c]	λ^{max}_{em} [nm]	Oscillator strength	Contribution[c]
BMeSA	306	0.151	H→L (0.69)	342	0.143	L→H (0.70)
	244	0.113	H→L+1 (0.68)			
1a	332	0.097	H→L (0.70)	366	0.098	L→H (0.68)
	283	0.666	H→L+1 (0.70)			
1b	383	0.038	H→L (0.70)	535	0.038	L→H (0.68)
	314	0.66	H→L+1 (0.70)			
1c	416	0.022	H→L (0.70)	583	0.031	L→H (0.67)
	337	0.683	H→L+1 (0.70)			
1d	441	0.014	H→L (0.70)	688	0.019	L→H (0.68)
	356	0.600	H→L+1 (0.68)			

[a] Performed using the linear-response (LR) PCM method at the B3LYP/6-31+G(d,p) level. [b] Performed using the state-specific (SS) PCM method at the ωB97XD/6-31+G(d,p) level. [c] H: HOMO, L: LUMO. The contribution of each pair of molecular orbitals is given in parentheses.

As shown in Table 1, the wavelengths of the absorption and fluorescence spectra simulated by TD-DFT calculations are in the order of BMeSA < **1a** < **1b** < **1c** < **1d,** along with the HOMO-LUMO energy gaps. The main absorption spectra of BMeSA and BMeSA-Ar **(1a-d)** consisted of two excited states: the first lowest energy corresponding to the HOMO-LUMO transition, and the second lowest energy corresponding to the HOMO-LUMO+1 transition. In BMeSA-Ar (**1a-d**), the oscillator strengths of the HOMO-LUMO transitions were markedly smaller than those of the HOMO-LUMO+1 transitions. Theoretically, a small HOMO–LUMO overlap leads to low oscillator strength. In fact, the HOMO-LUMO transitions of all the BMeSA-Ar compounds exhibited small orbitals overlaps in the order of **1d** < **1c** < **1b** < **1a,** owing to the electron-donating abilities of the aryl groups and the linkages through the nodal planes. In contrast, the HOMO-LUMO+1 transitions exhibited large oscillator strengths due to the large orbitals overlappings of HOMO-LUMO+1 in the BMeSA-Ar compounds. The calculated oscillator strengths decreased with the electron-donating abilities of the aryl groups in both absorbance and fluorescence. These results were in agreement with the experimental measurements (see below).

Absorbance, fluorescence, and electrochemical properties of BMeSA and BMeSA-Ar (1a-d) in dichloromethane: Demonstration of the decrease in the absolute HOMO-level-dependent HOMO-LUMO gap, according to the nodal arrangement. The experimentally observed absorption and fluorescence spectra supported our initial theoretical calculations, in that the longest-wavelength absorption and fluorescence maxima red-shifted in the order of BMeSA < **1a** < **1b** < **1c** < **1d** (Table 2 and Figure 4). The Hammett substituent constants, σ, of the substituents on the aryl groups are –H (σ = 0.00) < $–NH_2$ (σ = −0.66) < $–NMe_2$ (σ = −0.83),[23] and the julolidyl group is more electron-rich than $–NMe_2$.[24] These red-shifts are, therefore, an effect of the decreased HOMO-LUMO gap, along with the increased HOMO energies owing to the donation of electrons by the substituents. The absorption spectrum of all the molecules showed two peaks: the first excited state corresponding to the HOMO-LUMO transition and the second excited state corresponding to the HOMO-LUMO+1 transition. The absorbance at the second excited state was, in fact, more drastically red-shifted than that at the first excited state, as a result of which these two peaks overlapped in **1b-d** (Figure S9: see the peak separations in Supporting Information). Basically, importantly, the small shift in the HOMO-LUMO transition plays a key role in the large Stokes shift of 188 nm in **1d**. The absorption extinction coefficients and fluorescent quantum yields decreased with the electron-donating ability of the aryl group. As described in the theoretical calculation part, small HOMO–LUMO overlaps lead to small transition dipole moments on the part of the first excited states in BMeSA-Ar (**1a-d**).

Table 2. Absorption and fluorescence properties of BMeSA and BMeSA-Ar (**1a-d**) in dichloromethane.

	λ_{abs} / nm	ε / M^{-1} cm^{-1}	λ_{em} / nm[a]	Φ[b]
BMeSA	253, 324	8211, 5527	381	0.43
1a	279, 340	22287, 4457	409	0.12
1b	300, 360[c]	26285, 3298[c]	478	0.07
1c	321, 378[c]	28106, 2801[c]	533	0.07
1d	336, 401[c]	20042, 1904[c]	589	0.03

[a] Excitation at 350 nm. [b] Determined relative to quinine sulfate in 0.1 M H_2SO_4.[22] [c] Determined by peak separation.

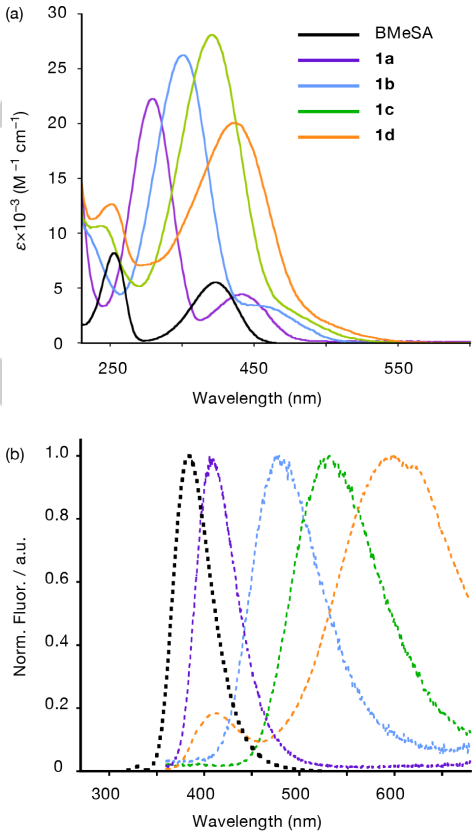

Figure 4. Absorption (a) and fluorescence (b) spectra of BMeSA and BMeSA-Ar (**1a-d**) in dichloromethane.

The cyclic voltammograms of BMeSA and BMeSA-Ar (**1a-d**) are shown in Figure 5. The HOMO energy levels of these molecules were estimated from their half-wave oxidation potentials; the HOMO–LUMO gaps were calculated from the absorption edges; and the LUMO levels were calculated by adding the HOMO–LUMO gaps to the values of the HOMO levels (Table 3). The HOMO levels were in the order of BMeSA > **1a** > **1b** > **1c** > **1d,** along with the electron-donating abilities of donor units. In contrast, the LUMO energies are nearly at the same levels. These results genuinely represent the control of the HOMO--level dependent energy gaps.

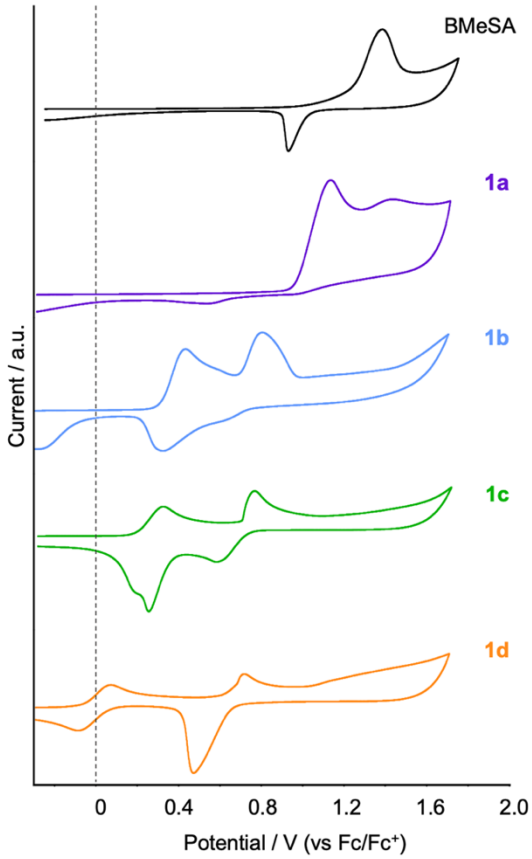

Figure 5. Cyclic voltammograms for the compounds BMeSA and BMeSA-Ar (**1a-d**) with 0.1 M solution of Bu_4NPF_6 in dichloromethane at room temperature relative to the Fc/Fc^+ couple.

Table 3. Electrochemical and photophysical data of BMeSA and BMeSA-Ar (**1a-d**) in dichloromethane.

	$E_{1/2}$ / V[a]	E_{HOMO} / eV[b]	E_{LUMO} / eV[c]	$E_{HOMO-LUMO}$ / eV[d]
BMeSA	+1.16	−5.96	−2.43	3.53
1a	+0.85	−5.65	−2.35	3.30
1b	+0.37	−5.17	−2.18	2.99
1c	+0.24	−5.04	−2.19	2.85
1d	+0.00	−4.80	−2.18	2.62

[a] Versus Fc/Fc^+. [b] Estimated from oxidation wave onset [HOMO = – ($E_{1/2}$ + 4.8 eV)]. [c] Calculated from the following equation: $E_{LUMO} = E_{HOMO-LUMO} + E_{HOMO}$. [d] Estimated from absorption edge.

Solvent effect on the absorbance and fluorescence spectroscopic properties of BMeSA and BMeSA-Ar (1a-d): Demonstration of a node-induced intramolecular charge transfer mechanism. The absorbance and fluorescence spectra of BMeSA and BMeSA-Ar **(1a-d)** are shown in Figure 6, and the fluorescence quantum yields are summarized in Table 4. No solvent effects were observed in the absorption spectra of BMeSA or BMeSA-Ar compounds. These molecules, therefore, adopt a non-polarized structure in the ground state. Conversely, typical solvatochromisms were observed in the fluorescence spectra of **1b-d**, which are categorized as positive solvatochromisms corresponding to a redshift with increasing solvent polarity. Therefore, these molecules adopt charge-polarized structures in the excited state, which can be stabilized by a polar solvent. Notably, no fluorescent solvatochromism was observed in BMeSA and **1a**, which have non-polarized structures in their excited states, suggesting that the electron-donating ability of the amino group is a key factor in the charge-polarized structure and the fluorescent solvatochromism. Indeed, the calculated dipole moments of BMeSA and **1a** in their excited states are small (1.3 and 4.9 D), whereas those of **1b-d** are large (18.3, 21.3, and 23.7 Debye) (Table 5).

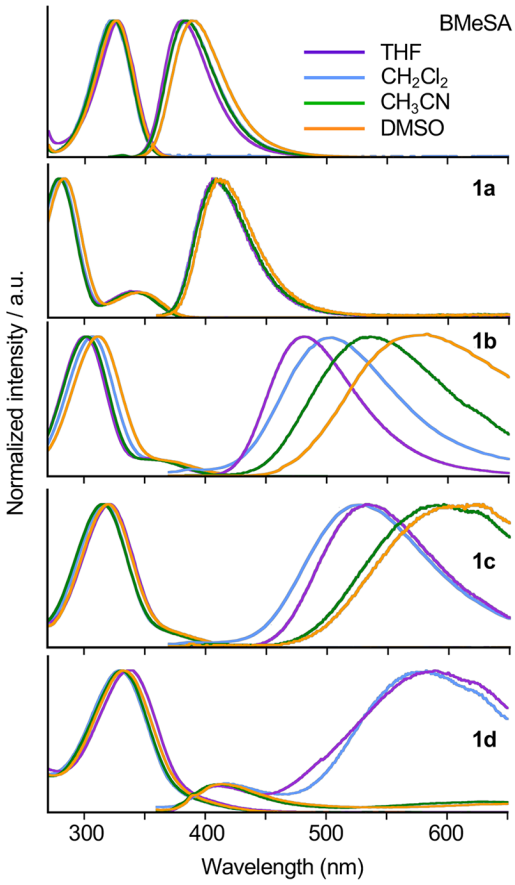

Figure 6. Absorption and fluorescence spectra of BMeSA and BMeSA-Ar (**1a-d**) in various solvents. The excitation wavelength was 300 nm. Fluorescence spectra of **1d** were normalized at 420 nm due to the small quantum yields of the intramolecular charge-transfer (CT) emission at longer wavelength.

Table 4. Fluorescence emission maxima and quantum yields of BMeSA and BMeSA-Ar (**1a-d**) in various solvents, and in solid-state.

	THF		CH_2Cl_2		CH_3CN		DMSO		Solid-State	
	λ_{em} / nm[a]	Φ[b]	λ_{em} / nm[a]	Φ[b]	λ_{em} / nm[a]	Φ[b]	λ_{em} / nm[a]	Φ[b]	λ_{em} / nm[d]	Φ[e]
BMeSA	384	0.55	381	0.43	384	0.38	388	0.59	387	0.12
1a	407	0.18	411	0.12	409	0.12	409	0.20	414	0.12
1b	505	0.07	478	0.07	538	0.02	570	0.01	484	0.08
1c	526	0.07	533	0.07	583	0.01	600	< 0.01	494	0.13
1d	590	0.03	589	0.03	-[c]	-[c]	-[c]	-[c]	544	0.01

[a] Excitation at 300 nm. [b] Determined relative to quinine sulfate in 0.1 M H_2SO_4.[22] [c] Not determined due to weak fluorescence intensities. [d] Excitation at 350 nm. [e] Determined in an integrating sphere.

It has been reported and widely observed in the category of push-pull type biphenyls that two factors are regarded as the electronic-coupling elements between the donor and acceptor subunits: (1) the torsion angle between aryl–aryl bonds, and (2) the linear combination of atomic orbitals (LCAO) coefficients of the $2p_z$ orbitals on the acceptor's LUMO and the donor's HOMO at the aryl–aryl bonds.[25] Interestingly, the excited-state geometries on the biphenyl moieties in **1b-d** were more planar than the ground-state geometries (Table 5). The fluorescent mechanism, therefore, appears to be based on PICT (planar intramolecular charge transfer). However, the fluorescence quantum yields markedly decreased with increasing solvent polarity. Compound **1d** exhibited dual fluorescence originating from two different CT states, where the 420 nm and 600 nm emission wavelengths were assignable to the BMeSA skeleton and the whole **1d** molecule, respectively.[26] These behaviors are commonly observed in TICT (twisted intramolecular charge transfer) mechanisms. The very weak molar extinction coefficients of **1b-d**, which correspond to the HOMO–LUMO transitions, also suggest a twisted geometry and poor orbital overlap. Generally, the contribution of the biaryl torsion effect to the charge separation is greater than that of the LCAO coefficients effect.[27] In BMeSA-Ar, however, the LCAO coefficients on the acceptor's LUMO were hindered by the nodal plane. Therefore, the small LCAO coefficients on the acceptor's LUMO influence the charge separation in the excited states of **1b-d**. This CT mechanism is different from that of both PICT and TICT and can be described as "node-induced intramolecular charge transfer." The fluorescence wavelengths and quantum yields in the solid-states were similar to those in less polar solvents, such as THF and dichloromethane (Table 4). In addition, the interplanar angles of the biphenyl groups in **1a-d** are in the range of 144.22°-167.58° are acceptable values for the orbital overlap between two benzene rings (Table 5). Moreover, no significant molecular stacking was observed in the crystal packings, except for the crystal of BMeSA (Figure S11: see the packing structures of BMeSA in Supporting Information). These results indicate that this charge separation system is effective in both the solution and solid-states without considering the molecular motion and intermolecular interactions.

Table 5. Calculated biaryl torsion angles and dipole moments of BMeSA and BMeSA-Ar (**1a-d**) in dichloromethane, and experimental data in the single crystals.

	Biaryl torsion angles / °			Dipole moments / Debye	
	GS[a]	ES[b]	Crystal[c]	GS[a]	ES[b]
BMeSA	-	-	-	0.688	1.317
1a	143.02	153.22	146.28	0.889	4.904
1b	144.53	164.05	152.64	3.545	18.30
1c	146.43	164.65	144.22	4.658	21.16
1d	146.60	164.68	167.58	4.653	23.69

[a] Performed by ground state (GS) geometry optimization with equilibrium solvation at the B3LYP/6-31+G(d,p) level. [b] Performed by the equilibrium solvation state-specific calculation of the excited state (ES) at the ωB97XD/6-31+G(d,p) level. [c] Average values.

Origin of asymmetric molecular orbital distribution and nodal planes on BMeSA. To generate a nodal plane through the atoms on a benzene ring, it is necessary to resolve the orbital degeneracy of the HOMO and LUMO, where there are two units with the same energy level. As shown in Figure 7, the meta di-substituted benzene, with two electron-withdrawing groups, effectively generates the asymmetric molecular orbital distribution and nodal plane through atoms with sites that are available for modification. More importantly, the amino group of BMeSA plays a role in separating the energy between the HOMO and HOMO−1, and between the LUMO and LUMO+1. This makes BMeSA a promising candidate for use in fine-tuning the optical properties of organic molecules without the undesirable

exchange of energy levels between the LUMO and LUMO+1. If the differences in energies between the LUMO and LUMO+1 levels were small, the LUMO and LUMO+1 levels could be changed by the introduction of a π-conjugation unit at the free 4-position, due to the stabilization of the LUMO+1 level with a large orbital overlap. Conversely, the introduction of an acceptor-substituted Ar group, such as a 4-cyanophenyl or 4-formylphenyl group, is different from the introduction of the π-conjugation units and not acceptable for this system. DFT calculations suggested that the acceptor units lowered the LUMO+1 level significantly, leading to the change in the LUMO and LUMO+1 levels; subsequently the LUMO were distributed over the entire molecule (Figure S12: see the DFT calculations in Supporting Information). Consequently, the decrease in the absolute HOMO level-dependent HOMO-LUMO gap was not achieved in this case.

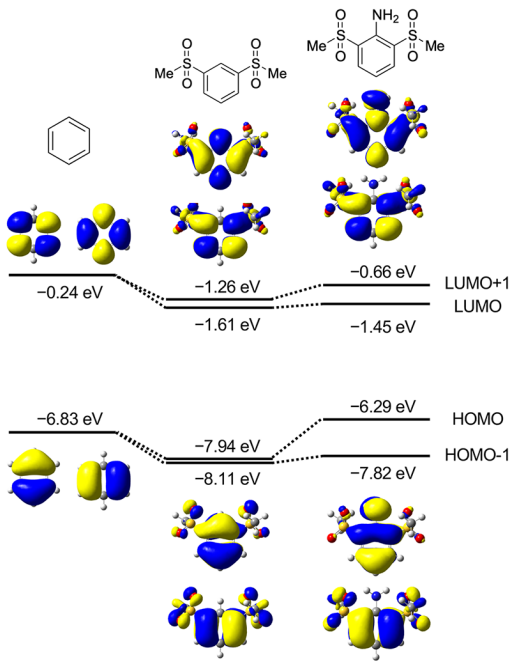

Figure 7. Frontier molecular orbitals and orbital energies of benzene, 1,4-bis(methylsulfonyl)benzene, and BMeSA calculated at B3LYP/6-31G(d) level in a gas phase.

Conclusions

Tuning the optical properties of sulfonylaniline fluorophores was demonstrated via asymmetric molecular orbital distribution and linkage through nodal planes. Controlling the HOMO-dependent energy gap was achieved by exploiting the strong orbital overlap in the HOMO, and the minimal orbital overlap in the LUMO. Furthermore, the nodal arrangement of the LUMO revealed a large excited-state dipole moment and influence on charge separation in the excited state, resulting in strong positive solvatochromism in the fluorescence spectra with a large Stokes shift. The mechanism of the node-induced intramolecular charge transfer (NICT) is different from that of ordinary PICT and TICT. The BMeSA skeleton is suitable and preferable for molecular orbital tuning via resolution of the benzene ring degeneracy and generation of a nodal plane. The chemical availability and reactivity of brominated BMeSA derivative, **5,** reveal its potential as a valuable synthetic intermediate for π-extension at the 4-position of BMeSA. Not surprisingly, a charge separation method is important for the material design of OLED and OPV materials. We believe that these findings will provide a rational approach to constructing a wide variety of π-conjugated molecules for photonic and optoelectronic applications.

.

Experimental Section

Synthesis and chemical characterization: All chemicals and solvents were reagent grade, except for tetrahydrofuran (THF), which was distilled before use. All reactions were performed in standard dry glassware under an inert nitrogen (N_2) atmosphere. Column chromatography was performed using Kanto silica gel 60N, spherical neutral, 40 - 100 μm. Thin-layer chromatography (TLC) was performed using Merck pre-coated aluminum sheets covered with 0.20 mm silica gel with a UV-fluorescent indicator (λ = 254 nm). Melting points were determined using a Sansyo SMP-300 apparatus. Nuclear magnetic resonance spectra were obtained using a JEOL JNM-ECX operated at 500 MHz for ^{1}H or 125 MHz for ^{13}C. The samples for NMR were dissolved in deuterated chloroform containing tetramethylsilane (TMS) as an internal reference; chemical shifts (δ) are reported in parts per million. Elemental analyses were performed on a Perkin Elmer 2400 Series II CHN/O elemental analyzer. IR spectroscopy was conducted using a Jasco FT/IR-460 plus instrument with on KBr (press). High-resolution field-deposition mass spectra (FD-HRMS) were obtained using a JEOL JMS-T100GCV instrument employing anthracene as an internal standard.

2,6-Bis(methylsulfanyl)nitrobenzene (3): Dimethyldisulfide (3.55 mL, 37.7 mmol) and sodium borohydride (1.43 g, 37.7 mmol) were added to DMF (30 mL) at 50 °C under an N_2 atmosphere. After 2 h of stirring, 2,6-difluoronitrobenzene (1.33 mL, 12.6 mmol) was added to the solution at 0 °C. The resultant solution was stirred for 1 day at room temperature under an N_2 atmosphere. The reaction was then quenched with water. The mixture was extracted with Et_2O, washed with water and brine, and dried over Na_2SO_4. After removal of the solvent, the residue was purified by column chromatography on silica gel with hexane-ethyl acetate (3:1) as the eluent to give **3** as a yellow solid (2.11 g, 78%).; m.p. 115.8 °C–117.6 °C; ^{1}H NMR (500 MHz, $CDCl_3$): δ 7.41 (t, J = 8.0 Hz, 1H, phenyl), 7.18 (d, J = 8.0 Hz, 2H, phenyl), 2.48 (s, 6H, CH_3); ^{13}C NMR (125 MHz, $CDCl_3$): δ 147.66, 132.84, 120.33, 118.23, 17.79 ppm; IR (KBr): v = 2981 (CH), 2924 (CH) cm^{-1}; HRMS (FD$^+$): *m/z* calcd for $C_8H_9NO_2S_2$ [M^+]: 215.00747; found: 215.00759; Elemental analysis calcd (%) for $C_8H_9NO_2S_2$: C 44.63, H 4.21, N 6.51, S 29.79; found: C 44.65, H 4.23, N 6.36, S 29.80.

2,6-Bis(methylsulfanyl)aniline (4): 10 wt% Pd/C (500 mg) was added to a solution of **3** (1 g, 4.65 mmol) in THF (15 mL) and ethanol (15 mL) under an N_2 atmosphere. The reaction mixture was then continuously shaken under an H_2 atmosphere (balloon pressure) for 24 h. The black suspension was filtered through celite and washed with CH_2Cl_2; the solvent was then removed under reduced pressure to give **4** as a colorless oil (800 mg, 93%).; ^{1}H NMR (500 MHz, $CDCl_3$): δ 7.29 (d, J = 8.0 Hz, 2H, phenyl), 6.67 (t, J = 8.0 Hz, 1H, phenyl), 4.93 (br, 2H, NH_2),

2.37 (s, 6H, CH_3) ppm; ^{13}C NMR (125 MHz, $CDCl_3$): δ 147.66, 135.88, 131.10, 124.30, 17.06 ppm; IR (NaCl): v = 3439 (NH), 3340 (NH), 3056 (CH), 2985 (CH), 2918(CH) cm^{-1}; HRMS (FD$^+$): *m/z* calcd for $C_8H_{11}NS_2$ [M^+]: 185.00329; found: 185.00326; Elemental analysis calcd (%) for $C_8H_{11}NS_2$: C 51.85, H 5.98, N 7.56, S 34.60; found: C 52.00, H 6.29, N 7.53, S 34.57.

2,6-Bis(methylsulfonyl)aniline (BMeSA): *m*-CPBA (65%) (4.81 g, 18.31 mmol) was added to a cooled solution (0 °C) of **4** (800 mg, 4.31 mmol) in CH_2Cl_2 (60 mL), and the resulting suspension was stirred for 24 h at 0 °C. The reaction was quenched with a saturated aqueous solution of Na_2SO_3, diluted with 3M NaOH, and the aqueous layer was extracted with CH_2Cl_2. The combined organic layers were washed with water and brine. After drying over anhydrous Na_2SO_4, the solvent was removed under reduced pressure to yield BMeSA as colorless crystals (770 mg, 72%).; m.p. 155.2 °C–162.9 °C; ^{1}H NMR (500 MHz, $CDCl_3$): δ 8.04 (d, J = 8.0 Hz, 2H, phenyl), 6.95 (t, J = 8.0 Hz, 1H, phenyl), 6.62 (br, 2H, NH_2), 3.11 (s, 6H, CH_3) ppm; ^{13}C NMR (125 MHz, $CDCl_3$): δ 145.37, 136.34 124.33, 116.92, 42.77 ppm; IR (KBr): v = 3465 (NH), 3362 (NH), 3005 (CH), 2925 (CH) cm^{-1}; HRMS (FD$^+$): *m/z* calcd for $C_8H_{11}NO_4S_2$ [M^+]: 249.01295; found: 249.01264; Elemental analysis calcd (%) for $C_8H_{11}NO_4S_2$: C 38.54, H 4.45, N 5.62, S 25.72; found: C 38.48, H 4.32, N 5.46, S 25.78.

4-Bromo-2,6-bis(methylsulfonyl)aniline (5): NBS (660 mg, 3.71 mmol) was added to a solution of BMeSA (770 mg, 3.09 mol) in DMF (30 mL), and the resulting solution was stirred for 24 h at room temperature. The mixture was poured into water, and the resultant precipitate was filtered. The cake was washed with water and dried *in vacuo* to give **5** as a white solid (1.00 g, 99%).; m.p. 204.7 °C–205.1 °C; ^{1}H NMR (500 MHz, $CDCl_3$): δ 8.13 (s, 2H, phenyl), 6.59 (br, 2H, NH_2), 3.11 (s, 6H, CH_3) ppm; ^{13}C NMR (125 MHz, $CDCl_3$): δ 144.31, 138.72, 126.19, 108.27, 43.01 ppm; IR (KBr): v = 3472 (NH), 3376 (NH) cm^{-1}; HRMS (FD$^+$): *m/z* calcd for $C_8H_{10}NO_4S_2Br$ [M^+]: 326.92346; found: 326.92348; Elemental analysis calcd (%) for $C_8H_{10}NO_4S_2Br$: C 29.28, H 3.07, N 4.27, S 19.54; found: C 29.27, H 3.01, N 4.24, S 19.64.

3,5-Bis(methylsulfonyl)-[1.1′-biphenyl]-4-amine (1a): A mixture of $Pd(PPh_3)_4$ (28 mg, 0.0244 mmol), **5** (100 mg, 0.305 mmol), 4,4,5,5-tetramethyl-2-phenyl-1,3,2-dioxaborolane (**6a**, 75 µL, 0.366 mmol), and K_2CO_3 (211 mg, 1.52 mmol) in a toluene-ethanol-water (15 mL, 10 mL, 2 mL) mixture was stirred at 60 °C for 24 h under an N_2 atmosphere. The reaction was then quenched with water. The mixture was extracted with CH_2Cl_2, washed with water and brine, and dried over Na_2SO_4. After removal of the solvent, the residue was purified by column chromatography on silica gel with dichloromethane-ethyl acetate (10:1) as the eluent to give **1a** as colorless solid (79 mg, 80%).; m.p. 219.3 °C–220.5 °C; ^{1}H NMR (500 MHz, $CDCl_3$): δ 8.31 (s, 2H, phenyl), 7.56 (AA′MM′X, 2H, phenyl), 7.46 (AA′MM′X, 2H, phenyl), 7.38 (AA′MM′X, 1H, phenyl), 6.64 (s, 2H, NH_2), 3.14 (s, 6H, CH_3) ppm; ^{13}C NMR (125 MHz, $CDCl_3$): δ 144.26, 137.51, 134.46, 130.78, 129.34, 128.22, 126.48, 125.12, 43.02 ppm; IR (KBr): v = 3472 (NH), 3372 (NH) cm^{-1}; HRMS (FD$^+$): *m/z* calcd for $C_{14}H_{15}NO_4S_2$ [M^+]: 325.04425; found: 325.04492; Elemental analysis calcd (%) for $C_{14}H_{15}NO_4S_2$: C 51.67, H 4.65, N 4.30, S 19.71; found: C 51.71, H 4.89, N 4.23, S 19.68.

3,5-Bis(methylsulfonyl)-[1,1′-biphenyl]-4,4′-diamine (1b): A mixture of $Pd(PPh_3)_4$ (56 mg, 0.0487 mmol), **5** (200 mg, 0.609 mmol), 4-(4,4,5,5-tetramethyl-1,3,2-dioxaborolan-2-yl)aniline (**6b**, 160 mg, 0.731 mmol), and K_2CO_3 (421 mg, 3.05 mmol) in toluene-ethanol-water (16 mL, 10 mL, 2 mL) mixture was stirred at 60 °C for 24 h under an N_2 atmosphere. The reaction was then quenched with water. The mixture was extracted with CH_2Cl_2, washed with water and brine, and dried over Na_2SO_4. After removal of the solvent, the residue was purified by column chromatography on silica gel with dichloromethane-ethyl acetate (1:1) as the eluent to give **1b** as a pale yellow solid (148 mg, 71%); m.p. 234.7 °C–237.2 °C; ^{1}H NMR (500 MHz, $CDCl_3$): δ 8.21 (s, 2H, phenyl), 7.36 (AA′XX′, 2H, phenyl), 6.75 (AA′XX′, 2H, phenyl), 6.53 (s, 2H, NH_2), 3.80 (br, 2H, NH_2), 3.13 (s, 6H, CH_3) ppm; ^{13}C NMR (125 MHz, $CDCl_3$): δ 146.67, 143.30, 133.47, 131.06, 127.60, 127.44, 125.02, 115.64, 42.94 ppm; IR (KBr): v = 3735 (NH), 3463 (NH) cm^{-1}; HRMS (FD$^+$): *m/z* calcd for $C_{14}H_{16}N_2O_4S_2$ [M^+]: 340.05515; found: 340.05526; Elemental analysis calcd (%) for $C_{14}H_{16}N_2O_4S_2$: C 49.40, H 4.74, N 8.23, S 18.84; found: C 49.26, H 4.59, N 8.15, S 18.57.

***N*$^{4'}$,*N*$^{4'}$-Dimethyl-3,5-bis(methylsulfonyl)-[1,1′-biphenyl]-4,4′-diamine (1c):** A mixture of $Pd(PPh_3)_4$ (77 mg, 0.0663 mmol), **5** (272 mg, 0.829 mmol), *N,N*-dimethyl-4-(4,4,5,5-tetramethyl-1,3,2-dioxaborolan-2-yl)aniline (**6c**, 164 mg, 0.995 mmol), and K_2CO_3 (573 mg, 4.14 mmol) in toluene-ethanol-water (22 mL, 14 mL, 3 mL) mixture was stirred at 60 °C for 24 h under an N_2 atmosphere. The reaction was then quenched with water. The mixture was extracted with CH_2Cl_2, washed with water and brine, and dried over Na_2SO_4. After removal of the solvent, the residue was purified by column chromatography on silica gel with hexane-ethyl acetate (1:1) as the eluent to give **1c** as a yellow solid (203 mg, 67%).; m.p. 267.1 °C–271.2 °C; ^{1}H NMR (500 MHz, $CDCl_3$): δ 8.23 (s, 2H, phenyl), 7.45 (AA′XX′, 2H, phenyl), 6.79 (AA′XX′, 2H, phenyl), 6.50 (s, 2H, NH_2), 3.13 (s, 6H, CH_3), 3.01 (s, 6H, CH_3) ppm; ^{13}C NMR (125 MHz, $CDCl_3$): δ 150.31, 142.89, 133.11, 131.08, 126.95, 124.94, 124.93, 112.72, 42.80, 40.43 ppm; IR (KBr): v = 3473 (NH), 3369 (NH) cm^{-1}; HRMS (FD$^+$): *m/z* calcd for $C_{16}H_{20}N_2O_4S_2$ [M^+]: 368.08645; found: 368.08638; Elemental analysis calcd (%) for $C_{16}H_{20}N_2O_4S_2$: C 52.15, H 5.47, N 7.60, S 17.40; found: C 52.04, H 5.34, N 7.50, S 17.63.

2,6-Bis(methylsulfonyl)-4-(2,3,6,7-tetrahydro-1*H*,5*H*-benzo[*ij*]quinolizin-9-yl)aniline (1d): A mixture of $Pd(PPh_3)_4$ (106 mg, 0.0914 mmol), **5** (250 mg, 0.762 mmol), 9-(4,4,5,5-tetramethyl-1,3,2-dioxaborolan-2-yl)-2,3,6,7-tetrahydro-1*H*,5*H*-benzo[*ij*]quinolizine (**6d**, 366 mg, 1.22 mmol), and K_2CO_3 (526 mg, 3.81 mmol) in a toluene-ethanol-water (20 mL, 13 mL, 3 mL) mixture was stirred at 60 °C for 24 h under an N_2 atmosphere. The reaction was then quenched with water. The mixture was extracted with toluene, washed with water and brine, and dried over Na_2SO_4. After removal of the solvent, the residue was purified by column chromatography on silica gel with dichloromethane as the eluent to give **1d** as a yellow solid (143 mg, 44%).; m.p. 153.7 °C–161.2 °C (decomp); ^{1}H NMR (500 MHz, $CDCl_3$): δ 8.18 (s, 2H, phenyl), 7.00 (s, 2H, phenyl), 6.47 (s, 2H, NH_2), 3.19 (t, J = 6.0 Hz, 4H, CH_2), 3.12 (s, 6H, CH_3), 2.80 (t, J = 6.5 Hz, 4H, CH_2), 1.99 (dd, J = 6.0, 6.5 Hz, 4H, CH_2) ppm; ^{13}C NMR (125 MHz, $CDCl_3$): δ 142.91, 142.61, 132.83, 131.42, 124.82, 124.62, 123.92, 122.00, 49.90, 42.82, 27.73, 21.89 ppm; IR (KBr): v =3643 (NH), 3360 (NH), 2927 (CH) cm^{-1}; HRMS (FD$^+$): *m/z* calcd for $C_{20}H_{24}N_2O_4S_2$ [M^+]: 420.11775; found: 420.11789; Elemental analysis calcd (%) for $C_{20}H_{24}N_2O_4S_2$: C 57.12, H 5.75, N 6.66, S 15.25; found: C 56.85, H 5.75, N 6.29, S 15.16.

Optical spectroscopy and electrochemical studies: All measurements were performed using Kanto HPLC grade solvents. UV/Vis spectra of solutions were obtained using a Hitachi U-2810 spectrophotometer (concentration: 10^{-4} M). Fluorescence spectra were obtained using a Shimadzu FR-6000 instrument (concentration: 10^{-5} M). Cyclic voltammograms (CVs) were recorded on an ALS electrochemical analyzer CH Model 612E in dichloromethane containing tetrabutylammonium hexafluorophosphate (Bu_4NPF_6, 0.1 M) as the supporting electrolyte at a scan rate of 100 mV/s. Counter and working electrodes were made of Pt, and the reference electrode was Ag/Ag$^+$. All potentials were calibrated versus a ferrocene standard.

Theoretical calculations of BMeSA derivatives: Ground-state geometry optimizations were performed at the B3LYP/6-31+G(d,p) level; Excited-state geometry optimizations were performed at the ωB97XD/6-31+G(d,p) level. The solvent models were introduced using the polarizable continuum method (PCM). Absorption properties were calculated using the linear-response (LR)[28,29] model at the B3LYP/6-31+G(d,p) level; emission property calculations were performed using the State-Specific (SS)[30] model at the ωB97XD/6-31+G(d,p) level. Ground-state dipole moments were determined by ground state geometry optimization with equilibrium solvation; excited-state dipole moments were determined by equilibrium solvation state-specific calculation of the excited state. Other proven functionals such as PBE0 and M06-2X were employed in the ground-state calculations; PBE0 and CAM-B3LYP were employed in the excited-state calculation (Table S2 and S3: see the DFT calculations in the Supporting Information).

Acknowledgements

This study was supported by the Naito Foundation (No. 287 to H.K.), a Grant-in-Aid for Scientific Research (C) (15K05468 to H.K.) from the Ministry of Education, Culture, Sports, Science and Technology (MEXT), and the YU-COE (M) program from Yamagata University (M30-5 to H.K.).

Keywords: Frontier molecular orbital • Degeneracy breaking • Nodal plane • Push–pull system • Sulfonylaniline

[1] L. D. Lavis, R. T. Raines, *ACS Chem. Biol.* **2008**, *3*, 142–155.
[2] H. Kobayashi, M. Ogawa, R. Alford, P. L. Choyke, Y. Urano, *Chem. Rev.* **2010**, *110*, 2620–2640.
[3] A. P. Kulkarni, C. J. Tonzola, A. Babel, S. A. Jenekhe, *Chem. Mater.* **2004**, *16*, 4556–4573.
[4] H. Sasabe, J. Kido, *Chem. Mater.* **2011**, *23*, 621–630.
[5] A. R. Murphy, J. M. J. Fréchet, *Chem. Rev.* **2007**, *107*, 1066–1096.
[6] C. Wang, H. Dong, W. Hu, Y. Liu, D. Zhu, *Chem. Rev.* **2012**, *112*, 2208–2267.
[7] F. Bureš, *RSC Advances* **2014**, *4*, 58826–58851.
[8] M. Kreyenschmidt, M. Baumgarten, N. Tyutyulkov, K. Müllen, *Angew. Chem. Int. Ed.* **1994**, *33*, 1957–1959.
[9] E. Maggio, N. Martsinovich, A. Troisi, *Angew. Chem. Int. Ed.* **2012**, *52*, 973–975.
[10] Y. Yamaguchi, K. Ogawa, K.-I. Nakayama, Y. Ohba, H. Katagiri, *J. Am. Chem. Soc.* **2013**, *135*, 19095–19098.
[11] Y. Yamaguchi, M. Takubo, K. Ogawa, K.-I. Nakayama, T. Koganezawa, H. Katagiri, *J. Am. Chem. Soc.* **2016**, *138*, 11335–11343.
[12] A. G. Crawford, A. D. Dwyer, Z. Liu, A. Steffen, A. Beeby, L.-O. Pålsson, D. J. Tozer, T. B. Marder, *J. Am. Chem. Soc.* **2011**, *133*, 13349–13362.
[13] L. Ji, A. Lorbach, R. M. Edkins, T. B. Marder, *J. Org. Chem.* **2015**, *80*, 5658–5665.
[14] L. Ji, R. M. Edkins, A. Lorbach, I. Krummenacher, C. Brückner, A. Eichhorn, H. Braunschweig, B. Engels, P. J. Low, T. B. Marder, *J. Am. Chem. Soc.* **2015**, *137*, 6750–6753.
[15] J. Merz, J. Fink, A. Friedrich, I. Krummenacher, H. H. Al Mamari, S. Lorenzen, M. Haehnel, A. Eichhorn, M. Moos, M. Holzapfel, et al., *Chem. Eur. J.* **2017**, *23*, 13164–13180.
[16] M. V. Ivanov, S. A. Reid, R. Rathore, *The Journal of Physical Chemistry Letters* **2018**, *9*, 3978–3986.
[17] M. R. Talipov, T. S. Navale, R. Rathore, *Angew. Chem. Int. Ed.* **2015**, *54*, 14468–14472.
[18] M. V. Ivanov, V. J. Chebny, M. R. Talipov, R. Rathore, *J. Am. Chem. Soc.* **2017**, *139*, 4334–4337.
[19] M. V. Ivanov, K. Thakur, A. Boddeda, D. Wang, R. Rathore, *J. Phys. Chem. C* **2017**, *121*, 9202–9208.
[20] T. Beppu, S. Kawata, N. Aizawa, Y.-J. Pu, Y. Abe, Y. Ohba, H. Katagiri, *ChemPlusChem* **2014**, *79*, 536–545.
[21] T. Beppu, K. Tomiguchi, A. Masuhara, Y.-J. Pu, H. Katagiri, *Angew. Chem. Int. Ed.* **2015**, *54*, 7332–7335.
[22] J. W. Eastman, *Photochemistry and Photobiology* **1967**, *6*, 55–72.
[23] C. Hansch, A. Leo, R. W. Taft, *Chem. Rev.* **1991**, *91*, 165–195.
[24] O. Kwon, S. Barlow, S. A. Odom, L. Beverina, N. J. Thompson, E. Zojer, J.-L. Brédas, S. R. Marder, *J. Phys. Chem. A* **2005**, *109*, 9346–9352.
[25] R. R. Dogonadze, A. M. Kuznetsov, T. A. Marsagishvili, *Electrochimica Acta* **1980**, *25*, 1–28.
[26] H. Tanaka, K. Shizu, H. Nakanotani, C. Adachi, *J. Phys. Chem. C* **2014**, *118*, 15985–15994.
[27] J. Herbich, A. Kapturkiewicz, *J. Am. Chem. Soc.* **1998**, *120*, 1014–1029.
[28] Roberto Cammi, A. Benedetta Mennucci, Jacopo Tomasi, *J. Phys. Chem. A* **2000**, *104*, 5631–5637.
[29] M. Cossi, V. Barone, *J. Chem. Phys.* **2001**, *115*, 4708–4717.
[30] R. Improta, V. Barone, G. Scalmani, M. J. Frisch, *J. Chem. Phys.* **2006**, *125*, 054103.

WILEY-VCH

ARTICLE

Entry for the Table of Contents

ARTICLE

Degeneracy breaking: The orbital degeneracy of benzene rings is resolved by biased push-pull system and asymmetric molecular orbital distribution. A linkage through the nodal plane provides HOMO-level-dependent tuning of the optical properties, a large dipole moment in the exited state, and positive solvatochromism in fluorescence with a large Stokes shift produced by a node-induced intramolecular charge transfer mechanism.

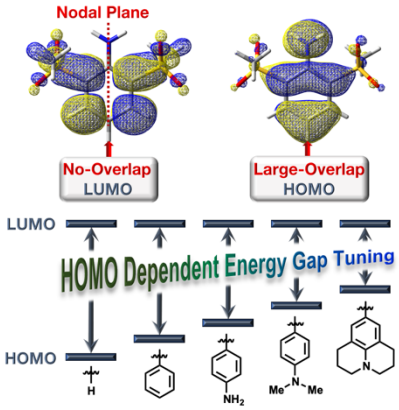

*Shoh Kudo, Nanami Hoshino, Teruo Beppu, and Hiroshi Katagiri**

Page No. – Page No.

Tuning the Optical Properties of Sulfonylaniline Derivatives: Degeneracy Breaking of Benzene Orbitals and Linkage Through Nodal Planes